Available online at www.sciencedirect.com

ScienceDirect

Physics Procedia 78 (2015) 230 – 239

Physics Procedia

15th Nordic Laser Materials Processing Conference, Nolamp 15, 25-27 August 2015, Lappeenranta, Finland

Towards a map of solidification cracking risk in laser welding of austenitic stainless steels

María-Asunción Valiente Bermejo[a]*, Tarasankar DebRoy[b], Kjell Hurtig[a], Leif Karlsson[a], Lars-Erik Svensson[a]

[a]*Department of Engineering Science, University West, Gustava Melins Gata 2, Trollhättan SE-461 86, Sweden*
[b]*Department of Materials Science and Engineering, The Pennsylvania State University, University Park, State College PA 16801, USA*

Abstract

In this work, two series of specimens with Hammar and Svensson's Cr- and Ni-equivalents (Cr_{eq}+Ni_{eq}) = 35 and 45 wt% were used to cover a wide range of austenitic grades. These were laser welded with different energy inputs achieving cooling rates in the range of 10^3 ºC/s to 10^4 ºC/s. As high cooling rates and rapid solidification conditions could favour fully austenitic solidification and therefore raise susceptibility to solidification cracking, the solidification modes of the laser welded specimens were compared to the ones experienced by the same alloys under arc welding conditions. It was found that high cooling rates experienced in laser welding promoted fully austenitic solidification for a wider range of compositions, for example specimens with (Cr_{eq}+Ni_{eq}) = 35% under arc welding cooling conditions at 10 ºC/s showed fully austenitic solidification up to Cr_{eq}/Ni_{eq} = 1.30, whilst the same specimens laser cooled at 10^3 ºC/s showed fully austenitic solidification up to Cr_{eq}/Ni_{eq} = 1.50 and those cooled at 10^4 ºC/s showed it up to Cr_{eq}/Ni_{eq} = 1.68. Therefore, high cooling rates extended the solidification cracking risk to a wider range of Cr_{eq}/Ni_{eq} values. This work also compares the cooling rates experimentally determined by thermocouples to the computed cooling rates calculated by a highly-advanced computational model. The distance between the thermocouple's wires and the thermal resistance of thermocouples together with the small size of the weld pools proved to be practical limitations in the experimental determination of cooling rates. However, an excellent agreement was found between computed and experimental solidus isotherms at high energy input settings. For low energy input settings cooling rate was in the order of magnitude of 10^4 ºC/s, whilst for high energy input settings cooling rate was found to be in the order of magnitude of 10^3 ºC/s.

Keywords: laser beam welding (LBW); Ytterbium fibre laser; austenitic stainless steel; ferrite; solidification modes; cooling rate.

Peer-review under responsibility of the Lappeenranta University of Technology (LUT)

* Corresponding author. Tel.: +34 667776172; *E-mail address:* asun.valiente@hv.se

Peer-review under responsibility of the Lappeenranta University of Technology (LUT)
doi:10.1016/j.phpro.2015.11.033

1. Introduction

About 1400 million tonnes of stainless steels are produced in the world per year and more than 50% are austenitic stainless steels. It is well recognised that laser beam welding is a very versatile joining process which can be easily automated and is capable to achieve high productivity and quality welds in different alloys. However, there are still some concerns about its use for welding of austenitic stainless steels.

Solidification cracking can be experienced by austenitic stainless steels during welding, in particular when weld solidifies exclusively as austenite. Causes have been extensively studied by Kujanpää et al. (1979, 1980, 1986), Kujanpää (1985), Lippold et al. (1982), Brooks (1992), Li et al. (1999) and Katayama et al. (1985) and it has been demonstrated that during fully austenitic solidification, impurities such as sulphur and phosphorus tend to segregate to the liquid phase and form low melting point eutectics. The distribution and nature of these eutectics along the grain boundaries at the last stages of solidification, together with the solidification shrinkage and the restraining forces are considered to be the main causes of solidification cracking. Therefore, solidification cracking is more likely for fully austenitic (A) and austenitic-ferritic (AF) solidification. In both solidification modes, austenite is the primary solidification phase, but in AF some ferrite is formed in the austenite boundaries because of the eutectic reaction experienced by the last-solidifying interdendritic liquid. Weld metals with primary ferritic solidification modes: ferritic-austenitic (FA) and fully ferritic (F) are less prone to solidification cracking because the solubility of impurities in ferrite phase is higher.

Laser beam welding (LBW), as a low energy input welding process can result in high cooling rates. It is well-known that high cooling rates can promote austenite as primary solidification phase. This phenomenon was observed and studied by Elmer et al. (1990, 1991), Lippold (1994), Fukumoto et al. (1998) and Iamboliev et al. (2003). Therefore, an austenitic alloy that under arc welding conditions solidifies as FA and does not present a risk of solidification cracking, when laser welded can shift to primary austenitic solidification and can become prone to cracking. Consequently, the study of the transition between primary austenitic and primary ferritic solidification modes is of utmost importance under low energy laser welding conditions.

Traditionally, the solidification mode has been related to the parameter chromium equivalent vs. nickel equivalent ratio Cr_{eq}/Ni_{eq}, (being Cr_{eq}= Cr + 1.37Mo and Ni_{eq}= Ni + 0.31Mn + 22C + 14.2N Hammar and Svensson's equivalents). However, it was recently found by Valiente Bermejo (2012-a) that the coexistence AF-FA depends also on the overall alloy content. For arc welding conditions and an overall alloy content of (Cr_{eq}+Ni_{eq}) = 30 wt%, the critical Cr_{eq}/Ni_{eq} ratio was between 1.38 and 1.55, while in case of (Cr_{eq}+Ni_{eq}) = 40 wt% the critical Cr_{eq}/Ni_{eq} ratio was between 1.28 and 1.32. Previous studies by Katayama et al. (1984), Elmer et al. (1989), Lippold (1994), Fukumoto et al. (1999) and Brooks et al. (2003) were conducted to investigate the effect of low energy welding processes on the transition between solidification modes but none of them considered the effect of the overall alloy content. Further information and comparison among Hammar and Svensson's equivalents and other Cr- and Ni-equivalents related to the transition between solidification modes and ferrite content prediction was published by Valiente Bermejo (2012-a, 2012-b, 2012-c).

Due to the experimental difficulties of measuring cooling rates in low energy laser welds, traditionally cooling rates have been estimated by different correlations such as the ones proposed by Flemings (1974), Esaka et al. (1988), Katayama et al. (1984) and Volkova et al. (2003). These correlations relate some thermal variables of the process with the resulting dendrite morphology, normally with the Dendrite Arm Spacing (DAS). However, in this study an attempt was made to measure cooling rates experimentally. In addition, an advanced computational method developed by one of the authors has been applied to calculate cooling rates.

Differently from previous work, the transition between solidification modes was evaluated at fixed overall alloy contents (Cr_{eq}+Ni_{eq}) and related to cooling rate. The combination of chemical compositions and cooling rates that cause fully austenitic solidification in the specimens evaluated, will serve as a basis to prepare a map of solidification cracking risk for laser welding of austenitics. This approach includes both the influences of the alloying content and the cooling rate and will thereby be of great help for the industry in project design stages.

2. Experimental work

2.1. Alloy selection

The overall alloy contents were fixed at (Cr_{eq}+Ni_{eq}) = 35% and at 45%. Eight samples with a fixed 35% alloy content but with Cr_{eq}/Ni_{eq} ratios from 1.23 to 2.04 were prepared and nine samples with a fixed 45% alloy content but with Cr_{eq}/Ni_{eq} ratios from 1.22 to 1.85. The range of ratios was selected so that the theoretical transition between solidification modes predicted by Katayama et al. (1984) was fully covered and included also lower and higher ratios. Each sample was prepared by melting combinations of gas tungsten arc (GTA) wires (AWS SFA5.9 ER310, ER312 and AWS SFA5.18 ER70S-6) with a total batch weight of 50 g using an electric arc furnace according to ASTM E1306-07 in a pure argon atmosphere. The final button-shaped alloys were cut and their chemical composition analyzed by Optical Emission Spectroscopy (Table 1).

Table 1. Chemical composition of the alloys (% wt)

Alloy	C	Mn	Si	S	P	Cr	Ni	N	Mo	Cr_{eq}/Ni_{eq}	Cr_{eq}+Ni_{eq}
1	0.114	1.63	0.55	0.007	0.017	19.303	12.356	0.029	0.084	1.23	35
2	0.088	1.63	0.55	0.006	0.017	19.587	12.024	0.046	0.081	1.30	35
3	0.100	1.65	0.54	0.006	0.017	20.127	11.307	0.041	0.077	1.39	35
4	0.095	1.66	0.53	0.006	0.016	20.636	10.728	0.039	0.073	1.49	35
5	0.119	1.67	0.53	0.006	0.015	20.625	10.047	0.043	0.069	1.50	35
6	0.099	1.68	0.54	0.005	0.015	21.604	9.540	0.045	0.064	1.68	35
7	0.107	1.71	0.53	0.005	0.017	22.640	8.240	0.054	0.056	1.91	35
8	0.105	1.73	0.53	0.006	0.018	23.232	7.610	0.069	0.051	2.04	35
9	0.095	1.65	0.449	0.005	0.019	24.411	16.804	0.050	0.108	1.22	45
10	0.099	1.67	0.439	0.004	0.018	24.752	16.339	0.050	0.105	1.26	45
11	0.099	1.66	0.448	0.004	0.019	25.042	16.014	0.051	0.103	1.30	45
12	0.102	1.66	0.445	0.005	0.019	25.422	15.512	0.064	0.100	1.33	45
13	0.117	1.68	0.442	0.005	0.019	25.788	15.126	0.055	0.097	1.36	45
14	0.098	1.69	0.449	0.005	0.020	25.990	14.969	0.077	0.096	1.39	45
15	0.111	1.72	0.438	0.004	0.018	26.799	13.754	0.063	0.089	1.53	45
16	0.113	1.76	0.438	0.003	0.018	28.108	12.274	0.080	0.079	1.72	45
17	0.133	1.76	0.435	0.004	0.019	29.196	10.961	0.097	0.071	1.85	45

2.2. Laser welding procedure

An Ytterbium Fibre Continuous Wave laser (YLR-6000-S) was used for laser welding of the specimens. Pure argon (99.997%) was used as shielding gas.

Some pre-trials were conducted in order to select the combination of laser variables with low (L) and high (H) energy inputs, which would ensure conduction and keyhole welding modes. Table 2 shows the final parameters and settings used for laser welding.

Table 2. Parameters and settings used in the laser welding

Settings reference	Energy input (J/mm)	Welding mode	Collimating (mm)	Focal length (mm)	Foc. pos. (mm)	Spot size in focus (mm)	Fiber ø (μm)	Nominal Power (W)	Welding speed (mm/s)
L	75	Conduction	200	200	0	0.8	800	750	10
H	110	Keyhole	160	300	0	1.125	600	2200	20

2.3. Cooling rate determination

Three different methods were used to determine cooling rates in the laser welds, i.e. an experimental determination by using thermocouples, a computational model that considers conduction and convection for the high energy input welds and finally a correlation based on the resulting dendrite morphology.

2.3.1. Experimental determination

Thermal cycles experienced during welding were recorded by K-type thermocouples (Nickel-chromium alloy/ Nickel-aluminium alloy) connected to a multi-channel thermocouples module that was regulated by a control system developed in-house and based on LabWIEW® programming. The temperature recording interval was set to 0.01 seconds.

Two commercial alloys were used: stainless steel alloy 304 (UNS S30400) representing the specimens whose alloy content is 35% whilst duplex stainless steel alloy 2205 (UNS S32205) represented the specimens with 45% alloy content.

Four experiments were conducted by combination of the two commercial alloys and the two welding settings (L and H described in Table 2): L-304, H-304, L-2205 and H-2205. Each welding experiment was repeated five times for data consistency and the results presented in the next section are representative for the thermal cycle of each experiment.

Each experiment included four different locations to register temperatures and six thermocouples. Figure 1 shows in full detail the thermocouples' location and references. At 0.5 mm below the surface in the centreline of the joint, one thermocouple (TC0) was located inside a 1.5 mm ø hole. On the top surface, at 1 mm distance from the centreline two thermocouples (TC2 & TC3) were placed, and also on the top surface but at 2 mm from the centreline two more thermocouples were located (TC1 & TC4). Finally, one thermocouple (TC5) was placed at the centreline of the joint on the top surface. It was decided to double the number of thermocouples initially planned on the top surface, to have better chances to get data at the designated locations.

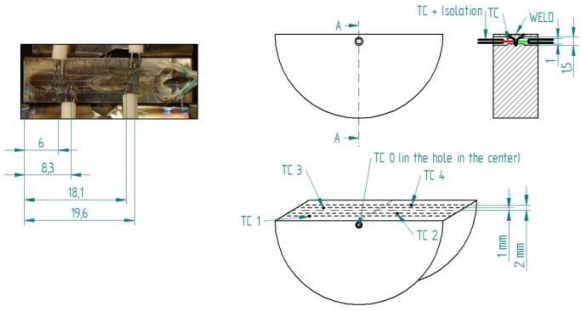

Fig. 1. Positioning and location of thermocouples.

2.3.2. Computational model

A heat transfer and liquid metal flow model was used to calculate temperature fields and cooling rates for the welding of 304 and 2205 stainless steels under the high energy input conditions (110 J/mm). The model has been extensively tested for the keyhole mode welding of Ta, Ti-6Al-4V, V, 304 stainless steel and a structural steel for various combinations of welding speed and power [by Rai et al. (2007a) and Rai et al. (2008)]. The different shape and size of the weld pool for different materials and welding conditions were satisfactorily predicted by the model. Welding conditions also represented different heat transfer mechanisms, i.e., conduction and convection dominated heat transfer modes in the weld pool. Computational efficiency of the numerical model was achieved by assuming a

quasi-steady state behavior of the keyhole shape and the flow of heat and liquid metal in the weld pool. A detailed description of the model is available in the literature [Rai et al. (2007b) and Ribic et al. (2011)].

2.3.3. Dendrite morphology correlation

As previously mentioned, some correlations were found for specific grades of stainless steels and are based on the relationship between some thermal variables of the process and the resulting dendrite morphology, normally the primary dendrite arm spacing (PDAS) and secondary dendrite arm spacing (SDAS). In this work, Katayama et al. (1984) correlation [SDAS= 25 $(C_R)^{-0.28}$] was used for cooling rate (C_R) estimation of alloys 304 and 2205.

2.4. Microstructural characterization

Once the specimens were laser welded they were cut and transverse cross-sections were ground and polished according to standard metallographic preparation procedures. The etchants used were Lichtenegger-Blöch (at 35-40ºC between 3.5 min. to 4 min.) and electrolytic etching (40% NaOH, 5V, 2 s). Optical microscopy (Leitz Aristomet, Olympus BX60M and Leica MEF4AM) was used for microstructural characterization.

3. Results and discussion

3.1. Cooling rates

It was not possible to obtain readings from the thermocouple placed in the centerline on the top surface in any experiment. It was intended to register temperatures upper solidus with that thermocouple, but the high heat density of the laser beam caused an immediate burn off of the thermocouple.

To avoid a direct contact between the thermocouple and the laser beam but to try to register temperatures in the melting range, a thermocouple was placed in the centerline of the joint but 0.5 mm below the surface. The distance below the surface was decided after a preliminary evaluation of the cross-section profiles of the laser welds, being 0.5 mm a convenient depth considering that average depths obtained with the low energy input settings was about 0.4 mm and with the high energy input about 2 mm. Therefore, it is expected that the thermocouple under the surface could be in contact with the molten metal in the welds prepared with the high energy input settings and that it could be very close to the molten metal or in the fusion boundary of the welds prepared with the low energy input settings.

Figure 2 shows the thermal cycles registered during laser welding of alloy 304, representing the 35% alloy specimens, under high (H) and low (L) energy input. For the low energy input experiments, all four thermocouples at a distance from the centerline gave readings, while for the high energy input experiments, the signal was lost in two of them but there were data from one thermocouple at each distance from the centerline.

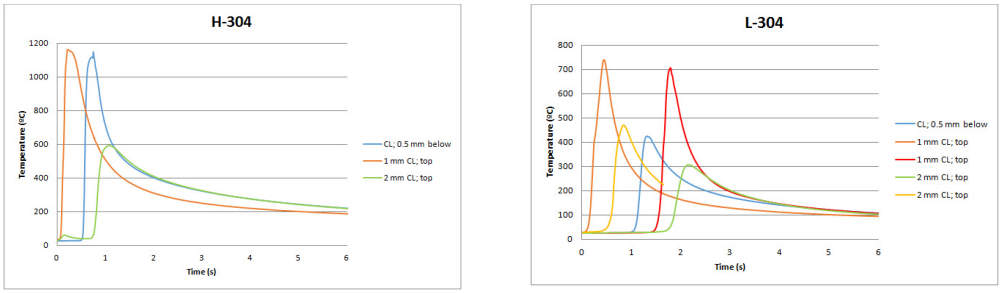

Fig. 2. Thermal cycles during welding of alloy 304. Left: High energy input (110 J/mm). Right: Low energy input (75 J/mm)

Figure 3 shows the thermal cycles registered during laser welding of alloy 2205, representing the 45% alloy specimens, under high and low energy input settings. In both experiments one thermocouple at a distance from the centerline was not giving any signal. A practical conclusion to be drawn from these experiments is the importance to

place more than one thermocouple in the designated positions to be studied, as there are several experimental reasons that may cause a failure in the thermocouple.

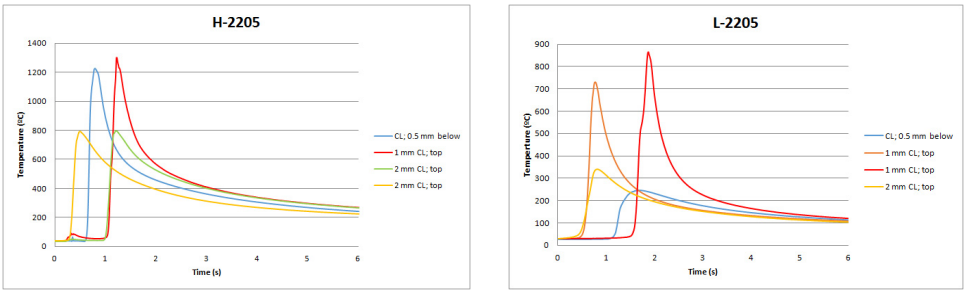

Fig. 3. Thermal cycles during welding of alloy 2205. Left: High energy input (110 J/mm). Right: Low energy input (75 J/mm)

Neither in the H experiment nor in the L experiment, was solidus temperature for alloy 304 (1400º C) or for alloy 2205 (1419ºC) registered by the thermocouples. In experiment H for alloy 304 (Fig.2), maximum temperatures registered were 1163ºC at 1 mm distance from the centerline on the top surface and 1148ºC at 0.5 mm below the surface in the centerline. These temperatures indicate that both locations were not melted and that they belong to or are very close to the fusion boundary, whilst in experiment L for alloy 304 (Fig.2), all temperatures registered indicate that locations are in the HAZ: thermocouples at 1 mm distance from the centerline registered the highest temperatures (738ºC and 706ºC), maximum temperature at 0.5 mm below the surface was 426ºC and at 2 mm from the centerline maximum temperatures were 306ºC and 471ºC.

Similarly, in experiment H for alloy 2205 (Fig.3), maximum temperatures registered were 1301ºC at 1 mm distance from the centerline on the top surface and 1224ºC at 0.5 mm below the surface in the centerline. These temperatures indicate that both locations belong to or are very close to the fusion boundary. In experiment L with alloy 2205, all temperatures registered indicate that measurement locations are in the HAZ (Fig.3).

Experimental cooling rates and computed cooling rates for alloy 304 (Cr_{eq}+Ni_{eq}=35%) at high energy input are shown in Table 3. A reasonable agreement was found between the experimental and computed cooling rates at 0.5 mm below the surface in the centerline. At 1 mm from centerline, they look quite similar to the computed cooling rates in the centerline in the range of temperatures between 500-927ºC and are in the range of magnitude of 10^3 ºC/s.

Experimental cooling rates and computed cooling rates for alloy 2205 (Cr_{eq}+Ni_{eq}=45%) at high energy input are shown in Table 4. There is a reasonable agreement between the experimental and computed cooling rates in the range of temperatures between 500-1127ºC and it is also in the range of magnitude of 10^3 ºC/s. Also an excellent agreement is found between computed and experimental solidus isotherms at high energy input settings for alloy 304 and alloy 2205 (Fig.4-5). The experimentally observed position of the fusion boundary should be compared to the combined maximum extent of the individual isotherms computed at different positions along the weld length.

According to both experimental cross-sections (Figs. 4-5), weld profiles were 2 mm depth and 3 mm width, which mean that the fusion boundary should be found at 1.5 mm from the centerline. Therefore, it was expected that the thermocouples in the centerline at 0.5 mm below the surface and at 1 mm from the centerline registered melting and even upper liquidus temperatures, but thermocouples located in those positions registered temperatures close to or in the fusion boundary. Some reasons might explain these differences, on one hand, the introduction of the hole for insertion of the thermocouple wires affects the local geometry of the weld pool, but more importantly, the practical attachment of the two wires composing a thermocouple involves a minimum separation of the wires that is typically 1-1.5 mm. It needs to be considered that in small laser weld pools like the ones presented in this study for H conditions (2 mm depth x 3 mm width) there is an average temperature gradient of about 900ºC/mm between the centre of the weld and the fusion boundary, but that is even more critical for the laser welds in L conditions (1.8 mm depth x 0.4 mm width), as the average temperature gradient is about 6600ºC/mm between the centre of the weld and the fusion boundary, therefore, a very short gap between the wires in the attachment of the thermocouples highly influences the temperature registered.

Table 3. Experimental and computed cooling rates for alloy 304 [Cr_{eq}+Ni_{eq}=35%] at high energy input settings

Type	Location	Cooling rates below solidus (ºC/s)				Cooling rate solidification (ºC/s)	Cooling rate upper liquidus (ºC/s)
		500-800ºC	800-927ºC	927-1127ºC	1127-1400ºC	1400-1454ºC	1454-1727ºC
Experimental	0.5 mm below surface, centerline	625	1963	1902			
Computed	0.5 mm below surface, fusion boundary	619	1171	1527	2126		
Computed	0.5 mm below surface, centerline	647	1238	1835	2698	444	2232
Experimental	1 mm from centerline, top surface	700	1345	854			
Computed	Fusion boundary, top surface	610	1062	2062	4064		
Computed	Centerline, top surface	647	1228	1821	3253	398	2037

Table 4. Experimental and computed cooling rates for alloy 2205 [Cr_{eq}+Ni_{eq}=45%] at high energy input settings

Type	Location	Cooling rates below solidus (ºC/s)				Cooling rate solidification (ºC/s)	Cooling rate upper liquidus (ºC/s)
		500-800ºC	800-927ºC	927-1127ºC	1127-1400ºC	1400-1454ºC	1454-1727ºC
Experimental	0.5 mm below surface, centerline	455	1444	2208	1104		
Computed	0.5 mm below surface, centerline	655	1234	1841	2681	637	2141
Experimental	1 mm from centerline, top surface	394	1234	1862	1620		
Computed	Fusion boundary, top surface	622	1108	1917	4522		
Computed	Centerline, top surface	647	1234	1793	3026	638	2110

Table 5 shows the cooling rates estimated by Katayama's correlation, and comparing them with the average values of experimental and computed cooling rates (Tables 3 and 4), they are in the same order of magnitude: about 10^3 ºC/s for the high energy input welds and about 10^4 ºC/s for the low energy input welds.

Table 5. Cooling rates estimated by Katayama's correlation

(Cr_{eq}+Ni_{eq})	Settings reference	SDAS (μm)	Cooling rate (C_R) (ºC/s)
35%	H	2.43+-0.46	4125
35%	L	1.76+-0.40	13056
45%	H	2.55+-0.40	3473
45%	L	1.60+-0.26	18350

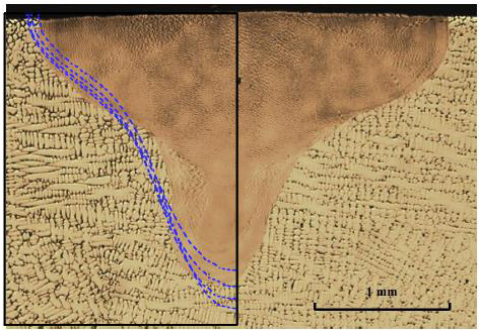

Fig. 4. Computed (blue lines) and experimentally determined transverse solidus isotherms for alloy 304 [Cr_{eq}+Ni_{eq}=35%] at high energy input settings. Each computed isotherm corresponds to a different position along the weld length.

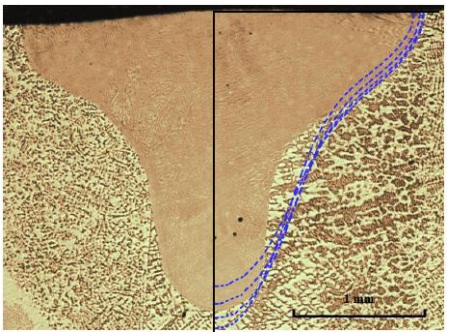

Fig. 5. Computed (blue lines) and experimentally determined transverse solidus isotherms for alloy 2205 [Cr_{eq}+Ni_{eq}=45%] at high energy input settings. Each computed isotherm corresponds to a different position along the weld length.

3.2. Solidification modes

Table 6 shows the solidification modes for the alloys (Cr_{eq}+Ni_{eq}=35% and 45%) prepared under three different conditions: first in a electric arc furnace cooled at 10 ºC/s (according to ASTM E1306-2007 at 30 V, 550A, 60 s melting time, 50 g of material, 3 min cooling time, Ar shielded), second, laser welded with high energy input settings cooled at about 10^3 ºC/s and third, laser welded with low energy input settings and cooled at about 10^4 ºC/s.

Table 6. Solidification modes of the alloys at the different cooling conditions

Alloy	Cr_{eq}+Ni_{eq}	Cr_{eq}/Ni_{eq}	10ºC/s	H (10^3 ºC/s)	L (10^4 ºC/s)	Alloy	Cr_{eq}+Ni_{eq}	Cr_{eq}/Ni_{eq}	10ºC/s	H (10^3 ºC/s)	L (10^4 ºC/s)
1	35	1.23	A	A	A	9	45	1.22	A	A	A
2	35	1.30	A	A	A	10	45	1.26	A/AF	A	A
3	35	1.39	AF/FA	A	A	11	45	1.30	AF/FA	A	A
4	35	1.49	AF/FA	A/AF	A/AF	12	45	1.33	AF/FA	A	A
5	35	1.50	AF/FA	A/AF/FA	A/AF/FA	13	45	1.36	AF/FA	A/AF	A/AF
6	35	1.68	FA	AF/FA	A/AF/FA	14	45	1.39	AF/FA	A/AF/FA	AF/FA
7	35	1.91	FA	A/AF/FA	AF/FA	15	45	1.53	FA	A/AF/FA	AF/FA
8	35	2.04	FA	FA/F	F	16	45	1.72	FA	FA	FA/F
						17	45	1.85	FA	FA/F	F

For Cr_{eq}+Ni_{eq}= 35% series and at arc furnace cooling conditions, fully austenitic solidification (A) is found in specimens up to Cr_{eq}/Ni_{eq}= 1.30, however, when laser welded fully austenitic solidification is found in a wider range of compositions, as it was found in specimens up to Cr_{eq}/Ni_{eq} =1.91. The same trend is observed for Cr_{eq}+Ni_{eq}= 45% series: fully austenitic solidification is found in specimens up to Cr_{eq}/Ni_{eq}= 1.26 under arc welding conditions, whilst in laser welded specimens the range of compositions is extended up to Cr_{eq}/Ni_{eq}= 1.53.

To illustrate the shift in the solidification modes caused by cooling conditions, figure 6 shows the AF/FA solidification modes in alloy 3 under arc furnace cooling conditions whilst figure 7 shows the fully austenitic solidification (A) in the same alloy but cooled at 10^3 ºC/s.

The shift in the solidification mode to primary austenitic under rapid cooling conditions was earlier documented in several studies [(Lippold et al. (1994), Fukumoto et al. (1998), Iamboliev et al. (2003), Elmer et al. (1990, 1991)]. The

stability of austenite as primary solidification phase increases compared to ferrite because of the increased dendrite tip undercooling, and in this work it was proved that laser welding and consequently higher cooling rates promoted fully austenitic solidification for a wider range of Cr_{eq}/Ni_{eq} ratios, and as previously mentioned in the introduction chapter, fully austenitic solidification makes the specimens susceptible to solidification cracking.

The experimental results presented in this work together with recent investigations involving more series of ($Cr_{eq}+Ni_{eq}$) values laser welded at different energy inputs will be a step forward towards the preparation of a map of solidification cracking risk in laser welding of austenitic stainless steels.

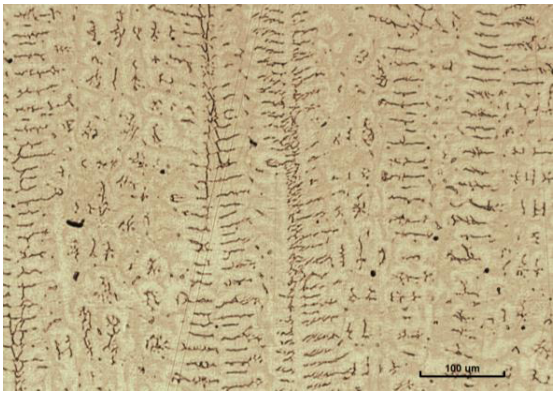

Fig. 6. Micrograph of alloy 3 arc welded (cooled at 10 ºC/s), showing coexistence between AF and FA solidification modes. Ferrite morphologies observed: eutectic ferrite (AF) (on the right of the image) and skeletal ferrite and a few traces of lathy ferrite (FA) (in the centre of the image).

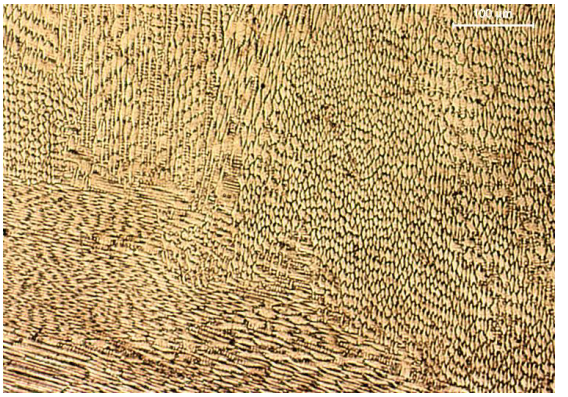

Fig. 7. Micrograph of alloy 3 laser welded (cooled at 10^3 ºC/s), showing fully austenitic (A) solidification mode. Cells and dendrites are the morphologies of austenite observed.

Another result worth noticing is that the coexistence AF-FA in arc welded specimens with $Cr_{eq}+Ni_{eq}$= 35% was observed at Cr_{eq}/Ni_{eq} ratios between 1.39 and 1.50 whilst for $Cr_{eq}+Ni_{eq}$= 45%, the coexistence is found at lower Cr_{eq}/Ni_{eq} ratios and at a narrower interval, from 1.30 to 1.39. This trend is in agreement with previous works involving other alloy contents (by Valiente Bermejo, 2012). However, when the same alloys experienced rapid cooling in laser welding, the coexistence takes place at higher Cr_{eq}/Ni_{eq} values, i.e., from 1.50 to 1.91 for 35% alloying content and from 1.39 to 1.53 for 45% alloying content.

4. Conclusions

- It was proved that high cooling rates promote fully austenitic solidification for a wider range of Cr_{eq}/Ni_{eq} values thereby making these alloys more susceptible to solidification cracking.
- At higher cooling rates, the transition between primary ferritic and primary austenitic solidification takes place at higher Cr_{eq}/Ni_{eq} values. However, the transition does not occur at a single Cr_{eq}/Ni_{eq} ratio and both solidification modes coexist in a range of Cr_{eq}/Ni_{eq} values.
- A reasonable agreement was found between the experimental, computed and dendrite morphology correlation methods for the high energy input settings: 10^3 ºC/s. Dendrite arm spacing was used in the estimation of cooling rates for the low energy welds and 10^4 ºC/s was the average value.
- Practical limitations were found in the experimental determination of cooling rates: the thermal resistance of thermocouples and the influence of the distance between the thermocouple's wires attachment on the temperatures registered.

Acknowledgements

Zhuyao Zhang at Metrode Products Ltd is gratefully acknowledged for the supply of the raw materials and for providing the electric arc remelting furnace to prepare the experimental alloys. Pere Armengol and Eduard Armengol at Servimp Armengol S.L. are especially thanked for their contribution to machining of the specimens. Kenneth Andersson at the Department of Engineering Science at University West is also gratefully acknowledged for his assistance during metallographic preparation and Josep A. Picas, Enric Martín and Maite Baile at CDAL-Universitat Politècnica de Catalunya are especially thanked for providing the equipment and facilities for metallographic inspection.

References

Brooks, J.A., 1992. Solidification behavior and cracking susceptibility of austenitic stainless steel welds, Proceedings of the 8th Annual North American Welding Research Conference, Columbus, USA.

Brooks, J.A., Robino, C.V; Headley, T.J; Michael, J.R., 2003. Weld solidification and cracking behavior of free-machining stainless steel. Welding Journal, num. 3, p. 51s-64s.

Elmer, J.W., Allen, S.M; Eagar, T.W., 1989. The influence of cooling rate on the ferrite content of stainless steel alloys. Proceedings of the 2nd International Conference on Trends in Welding Research, Gatlinburg, Tennessee, USA. ASM International, 165-170.

Elmer, J.W., Eagar, T.W., Allen, S.M., 1990. Single-phase solidification during rapid-resolidification of stainless steel alloys. Proceedings of the Materials Weldability Symposium. ASM International, Ohio, 143-150.

Elmer, J.W., Eagar, T.W., Allen, S.M., 1991. Modeling second-phase formation during rapid resolidification of stainless steel alloys. Conference on Stainless Steels, Chiba, Japan.

Esaka, H., .Mizoguchi, S., Kajioka, H., Senda, H., 1988. Relation Between Secondary Dendrite Arm Spacing and Cooling Rate for SUS304 Steel. CAMP-ISIJ 1, 268.

Flemings, M.C., 1974. Solidification of Castings and Ingots, in "*Solidification Processing*". In Flemings, M.C. Editorial McGraw-Hill, New York, chapter 5, p. 135-174.

Fukumoto, S., Kurz, W., 1998. Prediction of the δ to γ transition in austenitic stainless steels during laser treatment. ISIJ International 38, 71-77.

Fukumoto, S., Kurz, W., 1999. Solidification phase and microstructure selection maps for Fe-Cr-Ni alloys. ISIJ International 39, 1270-1279.

Iamboliev, T., Katayama, S., Matsunawa, A., 2003. Interpretation of phase formation in austenitic stainless steel welds. Welding Journal 82, 337s-347s.

Katayama, S., Matsunawa, A., 1984. Solidification microstructure of laser welded stainless steels. Proceedings International Congress on Applications of Lasers & Electro-Optics (ICALEO). Laser Institute of America 44, 60-67.

Katayama, S., Fujimoto, T, Matsunawa, A., 1985. Correlation among solidification process, microstructure, microsegregation and solidification cracking susceptibility in stainless steel weld metals. Transactions of Japanese Welding Research Institute 14, 123-138.

Kujanpää, V.P., Suutala, N, Takalo, T., Moisio, T., 1979. Correlation between solidification cracking and microstructure in austenitic and austenitic-ferritic stainless steel welds. Welding Research International 9, 55-75.

Kujanpää, V.P., Suutala, N, Takalo, T., Moisio, T., 1980. Solidification cracking - estimation of the susceptibility of austenitic and austenitic-ferritic stainless steel welds. Metal Construction 12, 282-285.

Kujanpää, V.P., 1985. Effects of steel type and impurities in solidification cracking of austenitic stainless steel welds. Metal Construction 17, 40R-46R.

Kujanpää, V.P., David, S.A., White, C.L., 1986. Formation of hot cracks in austenitic stainless steel welds- solidification cracking. Welding Journal 65, 203s-212s.

Li, L., Messler, R.W.Jr., 1999. The effects of phosphorus and sulphur on susceptibility to weld hot cracking in austenitic stainless steels. Welding Journal 78, 387s-396s.

Lippold, J.C., Savage, W.F., 1982. Solidification of austenitic stainless steel weldments: part III – The effect of solidification behavior on hot cracking susceptibility. Welding Journal 61, 388s-396s.

Lippold, J.C., 1994. Solidification behavior and cracking susceptibility of pulsed-laser welds in austenitic stainless steels. Welding Journal 73, 129s-139s.

Rai, R., Kelly, S.M., Martukanitz, R.P., DebRoy, T., 2008. A convective heat-transfer model for partial and full penetration keyhole mode laser welding of a structural steel. Metallurgical and Materials Transactions A 39A, 98-112.

Rai, R., Elmer, J.W., Palmer, T.A., DebRoy, T., 2007. Heat transfer and fluid flow during keyhole mode laser welding of tantalum, Ti-6Al-4V, 304L stainless steel and vanadium. Journal of Physics D: Applied Physics 40, 5753-5766.

Rai, R., Roy, G.G., DebRoy, T., 2007. A computationally efficient model of convective heat transfer and solidification characteristics during keyhole mode laser welding. Journal of Applied Physics 101, 054909-1/054909-11.

Ribic, B., Tsukamoto, S., Rai, R., DebRoy, T., 2011. Role of surface active elements during keyhole mode laser welding. Journal of Physics D 44.

Valiente Bermejo, M.A., 2012-a. Influence of the [Cr_{eq}+Ni_{eq}] alloy level on the transition between solidification modes in austenitic stainless steel weld metal. Welding in the World 56, num. 11-12, 2-14.

Valiente Bermejo, M.A., 2012-b. A mathematical model to predict delta-ferrite content in austenitic stainless steel weld metals. Welding in the World 56, num. 9-10, 48-68.

Valiente Bermejo, M.A., 2012-c. Predictive and measurement methods for delta-ferrite determination in stainless steels. Welding Journal 91, 113s-121s.

Volkova, O., Heller, H.P., Janke, D., 2003. Microstructure and Cleanliness of Rapidly Solidified Steels. ISIJ International 43, 1724-1732.